A Molecular Dynamics Study of Allosteric Transitions in Leishmania mexicana Pyruvate Kinase

A Molecular Dynamics Study of Allosteric Transitions in Leishmania Mexicana Pyruvate Kinase.

Ankita Naithani[1], Paul Taylor[1], Burak Erman[2*] and Malcolm D. Walkinshaw[1*]

[1] The Centre for Translational and Chemical Biology, School of Biological Sciences, The University of Edinburgh

[2] Department of Chemical and Biological Engineering, Koç University, Sariyer34450, Istanbul, Turkey

[*]Corresponding authors m.walkinshaw@ed.ac.uk and berman@ku.edu.tr

Short Title: The Allosteric Mechanism of Pyruvate Kinase

Key Words: fructose-2,6,-bisphosphate, allosteric activator, homo-tetramer enzyme, Monod-Wyman-Changeux mechanism

Abstract:

A comparative molecular dynamics analysis of the pyruvate kinase from Leishmania mexicana (LmPYK) is presented in the absence and presence of the allosteric effector fructose 2,6-bisphosphate (F26BP). Comparisons of the simulations of the large 240 kDa apo and holo tetramers show that binding of F26BP 'cools' the enzyme and reduces dynamic movement, particularly of the B-domain. The reduced dynamic movement of the holo form traps the PYK tetramer in its enzymatically active state with the B-domain acting as a lid to cover the active site. The mobile active-site α6' helix also undergoes a transition from helix (active R-state) to coil (inactive T-state). Analysis of the rigid body motions over the trajectory highlights the concerted anti-correlated rigid body rocking motion of the four protomers which is identified as a possible driver for the T to R transition. The transitions observed in these simulations are generally consistent with the Monod-Wyman-Changeux (MWC) model for allosteric activation but also suggest that rigidification or 'cooling' of the overall structure upon effector binding plays an additional role in enzyme activation.

INTRODUCTION

Pyruvate kinases are homotetrameric enzymes that catalyze the final reaction of glycolysis in which phosphoenolpyruvate and ADP are converted into pyruvate and ATP. The single chain PYK protomers are 50–60 kDa depending on species and are composed of four distinct domains. The active site is located in a cleft between the mobile B-domain and the end of the $(\alpha / \beta)_8$ -barreled A-domain of each of the four protomers (Fig. 1). The enzymatically active PYK tetramer has approximate dihedral symmetry (point group D2) with three orthogonal 2-fold axes relating the four protomers to each other. Crystallographic analyses of mammalian, bacterial, fungal and trypanosomatid PYKs all show a similar architecture [1] with the tetramer comprising a 'dimer of dimers' resulting in one large A-A interface (between the A-domains) and one small C-C interface between the C-domains (Figure 1).

Figure 1 Molecular architecture of pyruvate kinase

Figure 1. Left panel. Tetrameric form of LmPYK showing the four single chain protomers Oxalate and fructose-2,6-bisphosphate are shown as spheres occupying the active site and effector site respectively. The vertical and horizontal lines show the large (A-A) and small (C-C) interfaces. Right panel. The N-terminal domain (green), B-domain (red), A-domain (purple) and C-domain (orange) are highlighted for one of the protomers.

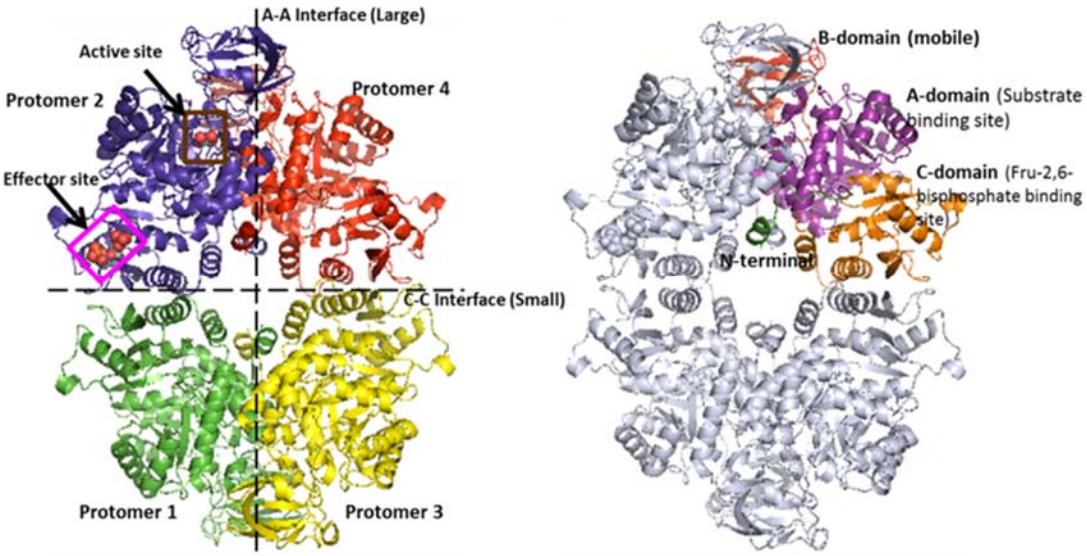

The allosteric behaviour is regulated by the effector molecule fructosebisphosphate (FBP) which binds to the C-domain of each protomer close to the small C-C interface of the tetramer. The question we address in this paper is how binding of FBP at a site over 40Å from the active site results in a 7 to 10 fold increase in activity (depending on species). Despite the structural similarities between the tetrameric PYK enzymes from the different families, there are very distinct differences in allosteric mechanisms. For example, the effector molecule for the trypanosomatid PYKs is fructose-2,6-bisphosphate (F26BP) while the effector for bacterial and mammalian PYKs is fructose-1,6-bisphosphate (F16BP). Such structural differences result in lower amino acid sequence identity around the effector binding site. Also there is biophysical evidence to show that regulatory mechanisms can vary and human M2PYK (one of the four human PYK isoforms) for example dissociates from active tetramer to inactive monomers as a control mechanism[2]. There is no evidence that any of the other PYKs use this as a regulatory control mechanism.

In this paper we present a comparative molecular dynamics (MD) analysis of the pyruvate kinase from Leishmania mexicana, LmPYK in order to study the effect of ligand binding on local and global dynamics of the tetramer. LmPYK was chosen as a model to study the allosteric activation of PYK as it is the only example of an allosteric enzyme where X-ray structures for all four relevant states are available; namely a T-state apo structure with no ligands bound; a structure in which only the effector molecule (F26BP) is bound; a substrate-only structure and a fully liganded structure with both substrate analogue and effector bound[1]. Overlays of the tetramers for each of these structures showed that only the unliganded T-state tetramer adopted a significantly different conformation from the other three R-state structures which have very similar (RMSFIT < 1 Å) conformations. The conformational transitions observed on going from the T to R state preserved the approximate D2 symmetry of the tetramer but involved changes in the relative orientations of the protomers and also changes in the inter-protomer interactions across the A-A and C-C interfaces. The major differences between the T and R state structures can be described as rigid-body rotations of the protomer domains and led to a description of the ~~a~~ 'rock-and-lock' mechanism for allosteric activation of LmPYK [1].

The 'rock-and-lock' mechanism fits with the original Monod-Wyman-Changeux (MWC) ideas of an essentially two- state equilibrium between inactive T-states and active R-states as observed

experimentally in a number of protein X-ray structures [3]. Despite the insight obtained from the R and T state LmPYK X-ray structures there are still some unanswered questions about the mechanism by which the enzyme shifts between the "off" and "on" states and in particular how the activity of the enzyme is altered by the binding of regulatory molecules. In this regard it is intriguing to note from the X-ray structures that the bound F26BP effector molecules do not make inter-protomer contacts. Instead, they bind to a flexible loop region. Experimentally it was found from thermal denaturation studies [1] that binding of the effector to LmPYK significantly increased the thermal melting temperature of the protein and the suggestion has been made that the approximately 7-fold increase of the catalytic rate of LmPYK upon F26BP binding is caused by a rigidification of the enzyme. Molecular dynamics (MD) provides an ideal tool to explore this possible mechanism.

Here we describe two MD simulations for the complete tetramer; the first in the absence of F26BP (the apo structure); the second with F26BP bound, (the holo structure). MD simulations of the isolated monomer are also described. The term 'protomer' refers here to a PYK chain when it is bound in the tetramer while 'isolated monomer' refers to a single PYK chain surrounded by solvent. The comparison of the apo and holo MD simulations identifies allosterically regulated movements of the tetramer as induced by F26BP binding. The time of the MD simulations (< 100ns) is too short to observe R to T transition, however, comparison of correlation of reside fluctuations from the tetramer and monomer trajectories show the role of thermal fluctuations on the individual domains of the protomers as well as providing insight into conformational transitions of the tetramer. The 'cooling' effect of F26BP binding which causes a general reduction in protein flexibility is also analysed. These thermodynamic effects along with specific structural rearrangements provide a detailed picture of the allosteric mechanism of LmPYK.

MATERIALS AND METHODS

In the Leishmania mexicana parasite, the four domains of pyruvate kinase are; the N terminal domain which is composed of residues 1-17, the A-domain which comprises residues 18-88 and 187-356; the B- domain which forms the mobile lid comprises residues 89-186 and the C-domain which incorporates the effector site and comprises residues 357-498.

A detailed comparison of the low resolution 3HQQ structure with 3HQN (unliganded LmPYK in the T-state) and 3HQP (LmPYK in complex with F26BP, ATP and oxalate) is given in the

Supplementary material. It can be seen from Figure S1 and Table S1 that despite the low resolution of 3HQQ, the structure provides clear experimental evidence for the 'R-like' conformational state of the F26BP effector-bound tetramer. The conformation of the 3HQQ tetramer (chains DEFG) was taken as a starting point for both an effector bound (LmPYK-F26BP) tetramer simulation and (by removing F26BP) a ligand-free LmPYK simulation. Comparison of these two simulations provides a useful insight into the nature of the effector-regulated T to R transitions.

In order to understand the extent of neighboring protomer effects, additional simulations were performed for isolated monomers from the apo and holo structures. Any monomer simulations used protomers extracted from the relevant tetramer X-ray structure.

All the MD simulations were carried out using GROMACS (GROningen MAchine for Chemical Simulations) package version 4.5[4] with AMBER99sb-ildn[5] force-field parameter set to model protein and small molecule effector and substrate molecules including F26BP and ATP. The starting structures were solvated in a dodecahedron box placed at a distance of 0.9 nm from the box boundary. Simple point charge (SPC) water molecules were used to fill the box, followed by the addition of sodium (Na^+) and chloride (Cl^-) ions to neutralize the system. The final systems contained approximately 84000 (monomer) and 300000 atoms (tetramer) with 76000 (monomer) and 272000 to 282000 (tetramer) water molecules respectively (Table 1). In order to maintain a constant temperature of 318 K, the protein and non-protein atoms were coupled to their own temperature baths using the V-rescale thermostat. This was followed by an NPT equilibration, in which the pressure was maintained isotropically at 1 bar using the Berendsen thermostat[6] with a coupling constant of 0.1 ps. For the apo simulation, the NPT equilibration was carried out for 250ps with 50,000 steps of 5 fs[4]. The holo equilibration was also carried out for 250 ps but using 62500 steps of 4fs. The NVT equilibrations were performed in the same way for 250ps but with 50,000steps at 5fs for the apo structure and 62500 steps at 4fs for the holo structure. It is known that the Berendsen thermostat does not generate a proper canonical ensemble however, such discrepancies are insignificant for large systems[7].

For all simulations the water molecules and bond lengths were restrained using the SETTLE[8] and LINCS[9] algorithms respectively. A single cut off of 1 nm was used for the treatment of Van

der-Waals interactions. Long-range electrostatic interactions were simulated using the Particle-Mesh Ewald (PME) method with 0.16 FF grid spacing and 4th order B-spline interpolation for the reciprocal sum space. The systems were relaxed by 1000 steps of steepest descent energy minimization procedure prior to the simulations. The snapshots were saved every 2ps, thereby yielding 10000-20000 frames (Table1). The use of the LINCS algorithm has been shown to allow simulations with an increased time step of up to 5fs[4], and this was used in the 78ns simulation of apo Lm PYK. Details of the time-steps and simulation times are summarized in Table 1.

Table 1: Description of the simulation parameters

Structure	Water atoms	Calpha atoms	System atoms	Time step (fs)	Number of frames	Simulation time (ns)
Holo Tetramer	272010	1992	305354	3	15642	48
Apo Tetramer	272043	1992	305251	5	16114	78
Holo Monomer	76353	498	84689	3	21764	65
Apo Monomer	76374	498	84676	5	10766	53

Periodic Boundary conditions were applied in all the directions. In the analysis of trajectories, the initial conformation for the tetramer, protomer and the isolated monomer were fixed and taken as the standard and all other conformations were expressed relative to this initial reference structure. RMSD plots for the apo and the holo structures are given in the Supplementary material section as Figures S2, S3, S4 and S5. Rigid body displacements and rotations were removed from all trajectories. Acpype[10] from AMBER was used to generate the topology of the ligand and PyMol[11] was used for generating the tetrameric structure. The computing resource used for this simulation was HecToR[12] Phase 3 service of Cray XE6 compute nodes consisting of two 2.3 GHz 16-core AMD Interlagos chips with a total of 2816 nodes.

RESULTS

Analysis of calculated and experimental B-factors

The motion of each atom appears as erratic fluctuations in the molecular dynamics trajectory. However, there are strong correlations between the motions of subsets of atoms and these collective protein motions may be extracted from the elements of the correlation matrix Each element of the matrix C_{ij} is obtained from the dot product $\langle \Delta R_i . \Delta R_j \rangle$ where ΔR_i and ΔR_j are the instantaneous fluctuation vectors of atoms i and j from their respective average positions over the time of the simulation. Only the C_α atoms are considered in this analysis. When the index i is equal to j, we obtain the mean squared fluctuations, $\left\langle \left(\Delta R_i\right)^2 \right\rangle$, of the residues, which may be compared with fluctuations obtained from the experimental B-factors determined by X-ray crystallographic refinement. Figure 2a shows the comparison between the measured B-factors from the apo X-ray structure (3HQN) and the calculated B-factors from the MD simulation of the apo tetramer. The experimental B-factors of 3HQN were transformed to mean-square displacement values using the expression: $\left\langle \left(\Delta R_i\right)^2 \right\rangle = \frac{3}{8\pi^2} B_i$. The resulting values were multiplied by the factor 318/100 to account for the temperature difference between experiment (100 K) and simulation (318 K).

Figure 2 Atomic fluctuations in pyruvate kinase.

Figure 2a :Comparison of experimental B-factors (red) from apoPYK (3HQN) with the mean square fluctuations of the Cα atoms of the LmPYK tetramer calculated from MD simulation (black). Both the representation of the tetramer (right) and the molecular cartoon (inset) highlight the mobile B-domains with dotted lines.
Figure 2b : Comparison of mean square fluctuations of the Cα atoms of the apo LmPYK tetramer (black) with the apo isolated monomer (red) calculated from MD simulation showing the enhanced mobility of the B-domain (residues 89-186) is even more exaggerated in the tetramer than the isolated monomer.
Figure 2c Mean square fluctuation comparison of apo LmPYK tetramer (average value 3.18 Å^2) and holo (F26BP)-bound tetramer (average value 2.81 Å^2).
Figure 2d: Differences in mean fluctuations for the isolated apo monomer (no F26BP bound; black) and the isolated holo monomer (with FBP bound; red).

Figure 2

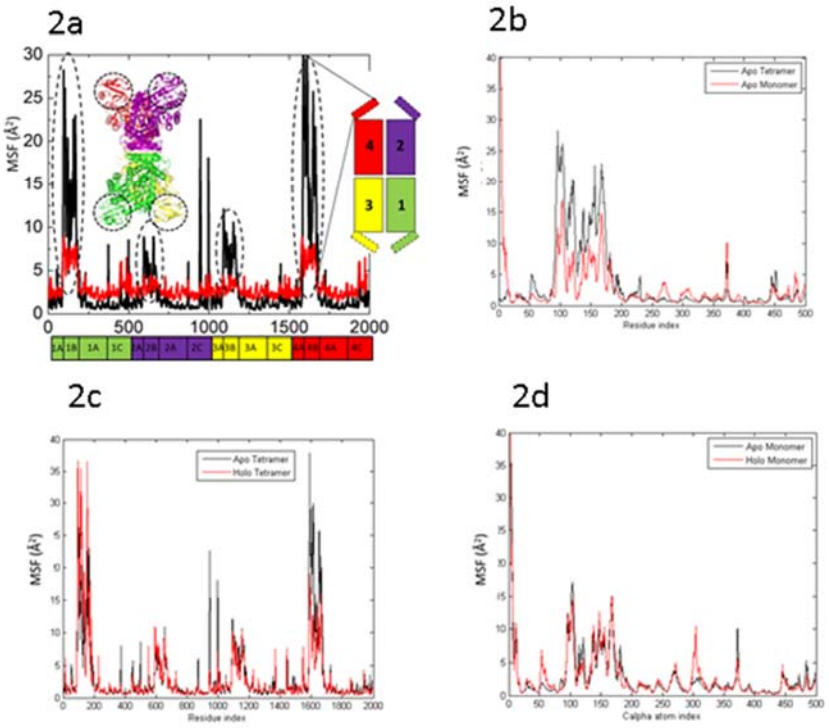

Comparison of the x-ray data and simulation results shows that the latter agrees quantitatively with experiment except the B-domain cap region, residues 89-186 (Figs. 1 and 2a), where simulation results show a much larger amplitude of motion compared to the x-ray structure. The larger fluctuation of the B-domain may plausibly be attributed to the aqueous environment in simulations in contrast to a more restrictive crystal environment. Indeed in a number of different crystal forms of PYK the B-domain is found to be totally disordered showing no interpretable electron density while the rest of the structure is well defined[1] suggesting that the B-domain can adopt multiple conformations even in crystal form.

The experimental Tm for apo LmPYK shows a partial melt at 313K and a complete melt at 323K. The holo structure show a single phase melt at the raised temperature of 335K. The simulations were carried out at 318K and the MSF analysis (Figure 2) supports the idea that

increased fluctuation of the B-domains and the effector loops may be responsible for the partial melt of apoLmPYK at the lower temperature of 313K.

What effect does constraining the PYK as a symmetrical tetramer have on the molecular flexibility? To answer this question we carried out MD simulations on an isolated monomer immersed in a water bath. A comparison of mean square fluctuation (MSF) values with the corresponding protomer chain locked in as part of a tetramer highlights the highly mobile B-domain movement in the tetramer simulation (Figure 2b). The enhanced mobility of the B-domain (residues 89-186) is also present in the isolated monomer simulation but is much-reduced with average MSF values for the B-domains alone of 13.8 $Å^2$ and 6.4 $Å^2$ for tetramer and monomer respectively. This rather unexpected result suggests that the B-domains behave differently (and are more mobile) as part of a tetramer.

We also compared molecular motion of the tetramer with and without the F26BP bound (Figure 2c). This showed that the apo structure fluctuates slightly more than the F26BP-bound holo tetramer with MSF values of 3.2 $Å^2$ and 2.8 $Å^2$ respectively. The simulation also shows an interesting asymmetry of movement of the B-domains which breaks the D2 symmetry of the tetramer; the B-domains (residues 89-186) of protomers 1, 2, 3, and 4 have MSF values of 13.8 $Å^2$, 4.7 $Å^2$, 6.6 $Å^2$, 16.5 $Å^2$ respectively. On binding the F26BP effector the MSF values change to 16.7 $Å^2$, 5.3 $Å^2$, 5.6 $Å^2$, 9.4 $Å^2$ respectively. However as observed experimentally in the X-ray structure (Figure 2a), the asymmetry of movement of the B-domains, with protomers 1 and 4 fluctuating more than protomers 2 and 3, is preserved in the apo and holo MD simulations.

Comparable simulations showing the effect of FBP on binding to the isolated monomer were also carried out (Figure 2d). MD simulations (~70ns) of the isolated monomer (residues 1-498) showed that the holo (F26BP bound) isolated monomer had small reduction of 0.08$Å^2$ over the 498 Cα atoms in MSF fluctuations compared with the isolated apo monomer.

Analysis of Correlation Matrices

The B-factors yield information on the fluctuations of the individual residues but do not contain information about the correlations between fluctuations of two different residues. The measure of correlation between the fluctuations ΔR_i and ΔR_j of i^{th} and j^{th} alpha carbons can be assessed by

calculating the projection of one on the other, i.e.,$\langle \Delta R_i . \Delta R_j \rangle$ at every instant and averaging over the full trajectory. The average, $\langle \Delta R_i . \Delta R_j \rangle$**,** if positive, indicates that the two residues move, on average, in the same direction. A negative correlation, or anti-correlation, indicates that the two atoms move in opposite directions. If two residues are displaced equally along the same direction, then their motions will be positively correlated and the distance between them will not change (as for example in a rigid body motion). If, on the other hand, two atoms move in opposite directions, their motion will be negatively correlated and the distance between them will either increase or decrease.

Anti-correlated residue motions and their changes upon effector binding provide significant information on the allosteric behavior of the LmPYK tetramer. The negative correlations of the apo-tetramer are visualised in Figure 3a by shading each anti-correlated residue pair. Shading is proportional to the magnitude of the anti-correlation and darker shaded regions correspond to groups or domains of anti-correlated residues. The white regions in Figure 3a correspond to protomer pairs with positive correlations. The numbering and the pairwise motions of the protomers for each shaded region are shown in Figure 3e. The tetramer consists of protomer 1 (residues 1-498), protomer 2 (499-997), protomer 3 (998-1496) and protomer 4 (1497- 1995). The clear block like pattern in Figure 3a shows that the protomers are moving in an anticorrelated fashion which is consistent with a concerted rocking motion depicted in Figure 3e and previously postulated in the 'rock-and-lock' mechanism identified from an analysis of crystal structures of the R and T-states of LmPYK [1]. (Though the anti-correlated movements identified in Figure 3 do not provide any evidence that these movements are concerted motions)

Figure 3: Correlated atomic motions in pyruvate kinase.

Negative correlations between atom pirs are plotted in Figures 3a and 3b with the maximum anticorrelation value scaled to -1 (black) and all other negative correlations shown on a shaded on a grayscale. All correlations greater than or equal to zero are white. Figure 3a. Negative correlations for the apo tetramer. Anticorrelations of allpairs of residues in the 4 protomers are plotted: protomer 1 (residues 1-498), protomer 2(499-997), protomer 3(998-1496) and protomer 4(1497- 1995). The block like pattern shows that the protomers are moving in an anticorrelated fashion. The dark regions result from fluctuations of the system with fixed centroid of the tetramer. Fluctuations of a protomer obtained by fixing its centroid shows correlations internal to the protomer, as depicted below in figures 3b-d.

Figure 3b. Negatively correlated regions of the apo protomer . Strongest anticorrelations are between the B-domain (residues (89-186)) and the N-terminal (1-89) and the C-domains (340-498).

Figure 3c. Differences in negative correlations of apo and holo protomer expressed as $\left\langle \left(\Delta R_i\right)^2 \right\rangle_{Holo} - \left\langle \left(\Delta R_i\right)^2 \right\rangle_{Apo}$ Dark regions show the decrease of negative correlations upon binding of the effector . This is consistent with effector binding dampening the motion of the B-domain.
Figure 3d. Differences in negative correlations of the isolated holo and apo monomer expressed as $\left\langle \left(\Delta R_i\right)^2 \right\rangle_{Holo} - \left\langle \left(\Delta R_i\right)^2 \right\rangle_{Apo}$. Dark regions show that negative fluctuations of the apo structure are much stronger than those of the holo structure. These responses are much less, however, than those observed in the protomer.
Figure 3e: Cartoon of the anti-correlated rocking motions of the 4 pyruvate kinase protomers (with residue numbering defined as in Fig. 3a).

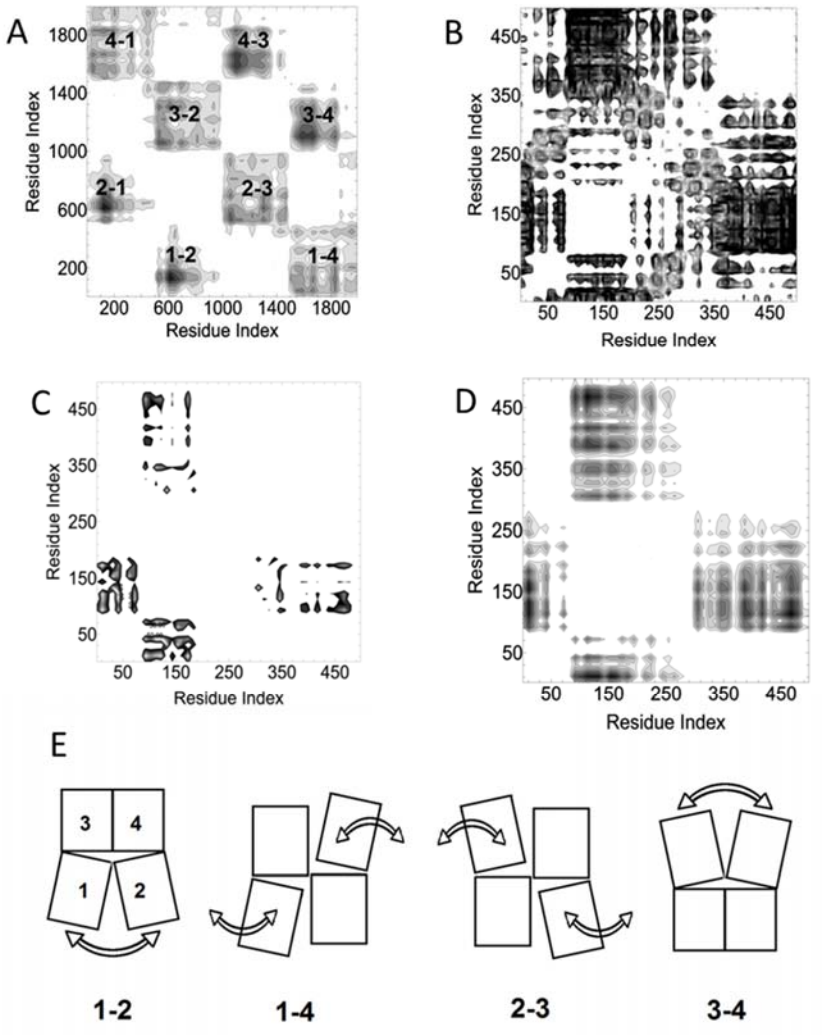

A more detailed analysis of the matrix showing anti-correlations in a single protomer within the tetramer is presented in Figure 3b, where the dark regions show the negatively correlated regions. The fluctuations of the centroid of the protomer have been removed from the trajectory

of the monomer, thus the calculated fluctuations are internal to the monomer. Strongest anti-correlations are between the B-domain (residues 89-186) and the N-terminal (1-89) and the C-domains (340-498). The change of correlations upon binding of the effector is of interest. In Figure 3c, the shaded regions identify those residues of the protomer where anti-correlations are either weakened or became positive upon binding of the effector. The weakened anti-correlated movements between the B-domain and the N-terminal residues and between the B and C domain residues are consistent with the interpretation from the temperature-factor analysis showing that effector binding dampens the motion of the B-domain. As an example, the negative correlation between residues Asn17 in the N-terminal and Lys118 in the B-domain is -15.0 $Å^2$ in the apo structure and reduces to -4.4 $Å^2$ upon effector binding. As another example, the negative correlation of -15.4 $Å^2$ between Glu156 in the B domain and Asn340 in the C domain of the apo structure reduces to -8.8 $Å^2$ upon effector binding. Since negative correlations result from the opening and closing of the B-domain cap, their decrease suggests that binding of the effector reduces the amplitude of the B-domain oscillations.

In order to study the effect of neighbouring protomers on the dynamics of the tetramer, simulations of the isolated holo and apo monomers in solution were also analysed. The differences of negative correlations between the isolated monomer holo and isolated monomer apo LmPYK chains are shown in Figure 3d. The shaded regions show that the anti-correlations of the apo structure are stronger than those of holo showing that binding of the effector decreases the negative correlations of the cap region and the effector binding region. This is a similar effect as shown from the tetramer simulation analysis (Figure3b) but now with a significantly reduced magnitude. We conclude that allosteric activity resulting from the anti-correlated behavior of the B-domain cap and the effector binding regions is already built into the isolated monomer, but is amplified by tetramer formation.

Pair-wise distance distributions identify differences in behaviour between the Apo and Holo structures

Molecular dynamics trajectories of the apo and the holo structures give information on how much time the system spends in a given conformational state[13]. Structural and dynamic differences in the apo and holo structures are analysed here using a novel plot of pair-wise distance distributions.

In order to track the interaction between a pair of residues over the course of an MD simulation the inter-atom distance is calculated at each time point and the frequency distribution of the distance is plotted over the time-course of the simulation. In many cases, as expected, the inter-residue distances show a normal distribution though frequently bimodal distributions or skewed distributions are observed. This graphical summary provides a convenient way of comparing the behaviour of holo and apo forms of LmPYK .

Activator binding changes residue fluctuations around the effector binding region: The ligand F26BP sits between two turn regions and interacts with Glu451 and Gly487. The distance between these two residues with F26BP bound is 12.0 Å as measured in the crystal structure. The MD simulation with F26BP removed (apo) shows a relaxation of the loop as shown by the increased inter-Cα distance between these two residues compared with the holo-structure (Figures 4a and 4b) Bound F26BP in the holo structure keeps the two residues close to the experimental X-ray distance with a mean distance of 12.5 Å while in the more flexible apo structure there is a broader almost bimodal distribution with preferred distances of 14.2Å and 17.5 Å (Figure 4b).

Figure 4: Selected pairwise distance distributions within a pyruvate kinase protomer showing conformational changes induced by F26BP binding.

Figure 4a: Cartoon of a pyruvate kinase protomer highlighting the residue pairs. 451-487;red, 261-264;yellow, 57-93; purple.
Figure 4b: Distribution of the distance between Glu451-Gly487 for the apo (black circles) and the holo (red circles) obtained from the MD trajectory. Inset figure shows conformations of the apo and holo tetramer. Apo is shown as a blue cartoon and the two residues are in stick representation in black. Holo is shown as a green cartoon with residues shown as red sticks.
Figure 4c: Distribution of the distance between His57-Gln93 for apo (black dots) and holo (red dots) obtained from the MD trajectory. Inset figure shows conformations of the apo and holo tetramer. Apo is shown as a blue cartoon and the two residues are in stick representation in black. Holo is shown as a green cartoon with residues shown as red sticks.
Figure 4d: Distribution of the distance between Ala261-Asp264 for apo (black dots) and holo (red dots) obtained from the MD trajectory. Inset figure shows conformations of the apo and holo tetramer. Apo is shown as a blue cartoon and the two residues are in stick representation in black. Holo is shown as a green cartoon with residues shown as red sticks.

Figure 4

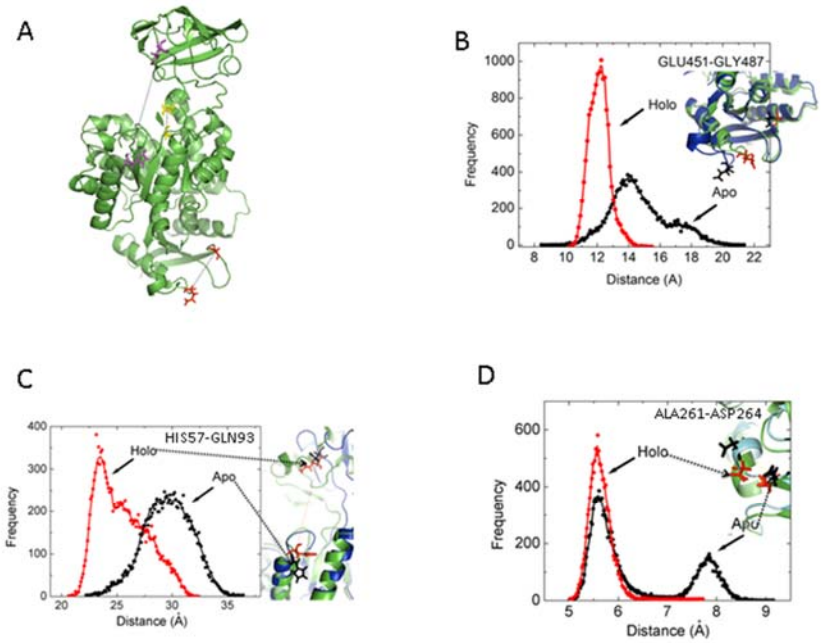

B-domain motion closes the active site. The largest movement in the enzyme ~~activity of PYK~~ is the opening and closing of the B-domain. This has been monitored by the inter-residue distance changes between residues of A (His 57; red) and B (Gln 93; green) domains for each protomer in the tetramer (Figure 4c). The mean distance in the apo tetramer (Figure 4c) is 30Å consistent with an open conformation of the B-domain (and which compares with an average distance in the apo crystal structure 3HQN of 27 Å). However, for the holo tetramer we see a bimodal distribution with a peak at 23Å and a shoulder at 28 Å which suggests that the bound F26BP is affecting the motion and open or closed state of the B-domain. For comparison, the X-ray structure of the ligand bound structure (3HQO) has four independent chains with the B-domains in partially closed states with corresponding distances ranging between 24 Å and 18 Å.

Monitoring distortions in the active site α6 helix: Ala 261 and Asp 264 are one helical turn apart in the short α6 helix which provides a crucial geometrical template for binding the substrate. The switch from the T to R states in LmPYK involves the rigid body rotation of the AC core[1]

which enables Arg310 on one protomer to form specific hydrogen bonds to the backbone carbonyls of arginine and glycine residues located in the α6' helix of the adjacent protomer. The short α6' helix (260-VAR**G**DL**G**VEIP-270) is unusual in that it contains two glycines. The MD simulation supports the idea that the allosteric mechanism may involve a transition between an ordered (R-state) helix able to bind substrate and a disordered (T-state) conformer. We observe a single, well-defined peak for the holo tetramer which corresponds with the ordered (R-state) helix. The apo tetramer however shows a bimodal distribution for the apo tetramer with peaks at 5.7 Å and 7.8Å (Figure 4d). These two peaks in apo tetramer suggest that the helix can distort and temporarily unwind in the absence of F26BP. Interestingly the Cα- Cα distance between A261 and D264 in structure 3HQQ used for MD is 6.5 Å while the corresponding distance in the apo-X-ray structure (3HQN) is 5.6 Å which closely agrees with the mean distance observed in the major peak in Figure 4d.

CONCLUSIONS

The MD simulations of tetrameric LmPYK in the apo and holo (F26BP-bound) states provide insight into the allosteric effector mechanism triggered by F26BP. By studying the dynamic behaviour of the tetramer compared with isolated monomer chains the simulations also show how the major allosteric effect is linked to a concerted motion of the complete tetramer. The analysis of correlated motion is consistent with a synchronised rocking of the protomers. There is a 12% in B-factor amplitude in the tetramer fluctuation on binding F26BP (which is at least in part due to a dampening of the B-domain movement). The reduced fluctuations in the tetramer may provide a mechanism which effectively cools down the tetramer and traps the tetramer in the active R-state conformation. This hypothesis is also consistent with the difference correlation plots which show that the magnitude of the anti-correlated movements, particularly involving the B-domain, are reduced on F26BP binding. Interestingly the behaviour of an isolated monomer PYK chain shows almost no effect on the overall B-factor upon F26BP binding, suggesting that the coupled movement of the protomers is required for this damping effect.

The concerted motions of the AC domains of the four protomers that make up each tetramer fit well with the classical Monod-Wyman-Changeux (MWC) model of allostery which suggests that oligomeric enzymes undergo symmetrical transitions (classically between the T- and R-states)

that can be stabilized by ligand binding [14]. However the asymmetric movements of the B-domains do not conform with the MWC requirement of perfectly conserved symmetry. Our observations showing a lowering of B-factors on effector binding might further suggest the effector is not only locking the R-state using local van der Waals and hydrogen bond interactions (as suggested previously [1]), but is also acting as a general heat-sink to cool down the whole tetramer. More recent descriptions of allostery highlight the role of entropy changes on effector binding[15,16] as well as the importance of the intrinsic dynamic nature of the protein[16,17]. Our observations on the effect of F26BP binding on ligand flexibility suggest that protein rigidity (related to melting temperature) and intrinsic heat capacity are important factors in stabilizing the R-state of PYK, and other allosteric proteins.

Another insight about the flexibility of PYK comes from a comparison of tetramer with the isolated monomer which shows that the B-domain in the tetramer is more mobile than in the isolated monomer. Interestingly, the B-domain movements in the tetramer have been frequently found to be asymmetric in a large number of PYK X-ray structures (e.g. PDB codes 1PKY, 1PKN, 1AQF, 1F3W)[18]. The asymmetry in these structures is such that B-domains of protomer pair 1 and 4 have similar B-factors and relative orientations which are frequently different from those of protomers 2 and 3 (protomer numbering as defined in Figure 3e). The asymmetry is sometimes imposed by the tetramer lying on a crystallographic 2-fold axis, but there are also many examples showing the same behaviour when there is no crystallographic constraint. The enhanced B-domain movement in the tetramer compared with the isolated monomer again suggests that interprotomer interactions regulate the pairwise B-domain movements. The strong anticorreation signals within each protomer (Figure 3) highlights the flapping of the B-domains though it is not clear mechanistically how the binding of the effector dampens the motion or how the synchronous movement of the B-domain pairs is regulated. The analysis of pairwise distance distributions is consistent with the results from the analysis of correlated motions in the tetramer and shows that F26BP binding not only restricts the mobility of the B-domain (as shown in Figure 4c) but also keeps the active site helix tight and the enzyme in an active R-state conformation (Figure 4d). This helical order-disorder transition between the T and R-states of LmPYK is key to explaining the on-off state of the enzyme as the phosphenoyl pyruvate substrate can only bind in the active site when the short α6'-helix (260-VAR**G**DL**G**VEIP-270) adopts an ordered conformation. That these MD simulations have captured this transition for the unliganded apo form

within the 80ns simulation indicates the relative instability of this glycine-rich helix. It is also significant in the simulations that the holo state is in the ordered (active R) state over the complete simulation while the apo (unliganded) can sample both disordered and ordered conformations (Figure 4d). These results suggest that the apo-enzyme can sample a range of conformational states, some of which would be similar to the active R-state. This dynamic description of PYK fits with the 'ensemble representation' and 'population shift' ideas of allosteric activation [16,19].

The MD analysis presented in this paper therefore supports a model in which concerted domain movements as described in the MYC model dominate the allosteric mechanism of LmPYK. However the analysis of specific order-disorder transitions and the 'heat-sink' effect of the bound effector highlight the importance of entropic and vibrational movements in regulating the allosteric effect of effector binding on the enzyme activity of leishmania pyruvate kinase.

Author Contributions

AN, PT and BE performed computational studies and analyzed data.
BE and MDW designed the research; analyzed data and wrote the paper.

Acknowledgements

We thank the British Council for grants to BE and MW. The computational work was supported by the Edinburgh Parallel Processing Facility and the Centre for Translational and Chemical Biology. AN was supported by the Darwin Trust.

1. Morgan H.P., I.W. McNae, M.W. Nowicki, V. Hannaert, P.A. Michels et al. (2010) Allosteric mechanism of pyruvate kinase from Leishmania mexicana uses a rock and lock model. J Biol Chem 285: 12892-12898.

2. Morgan H.P., F.J. O'Reilly, M.A. Wear, J.R. O'Neill, L.A. Fothergill-Gilmore, et al. (2013) M2 pyruvate kinase provides a mechanism for nutrient sensing and regulation of cell proliferation. Proceedings of the National Academy of Sciences.

3. Daily M.D., J.J. Gray (2007) Local motions in a benchmark of allosteric proteins. Proteins 67: 385-399.

4. Hess B., C. Kutzner, D. van der Spoel, E. Lindahl (2008) GROMACS 4: Algorithms for Highly Efficient, Load-Balanced, and Scalable Molecular Simulation. Journal of Chemical Theory and Computation 4: 435-447.

5. Lindorff-Larsen K., S. Piana, K. Palmo, P. Maragakis, J.L. Klepeis, et al. (2010) Improved side-chain torsion potentials for the Amber ff99SB protein force field. Proteins: Structure, Function, and Bioinformatics 78: 1950-1958.

6. Berendsen H.J.C.,J.P.M. Postma, W.F. van Gunsteren, A. Dinola, J.R. Haak, (1984) Molecular dynamics with coupling to an external bath. Journal of Chemical Physics 81: 3684-3690.

7. van der Spoel D., E. Lindahl, B. Hess, and the GROMACS development team (2014) GROMACS User manual version 4.6.6.

8. Miyamoto S., P.A. Kollman (1992) Settle: An analytical version of the SHAKE and RATTLE algorithm for rigid water models. Journal of Computational Chemistry 13: 952-962.

9. Hess B, H. Bekker, H.J.C. Berendsen, J.G.E.M. Fraaije, (1997) LINCS: A linear constraint solver for molecular simulations. Journal of Computational Chemistry 18: 1463-1472.

10. Sousa da Silva A., W. Vranken, (2012) ACPYPE - AnteChamber PYthon Parser interfacE. BMC Research Notes 5: 367.

11. DeLano W (2002) The PyMOL Molecular Graphics System.

12. Edinburgh Parallel Computing Centre (2007-2014) HECToR: UK National Supercomputing Service.

13. Wieligmann K, L.F.P. De Castro, M. Zacharias, (2002) Molecular Dynamics Simulations on the Free and Complexed N-Terminal SH2 Domain of SHP-2. In Silico Biology 2: 305-311.

14. Monod J., J. Wyman, J-P. Changeux, (1965) On the nature of allosteric transitions: A plausible model. Journal of Molecular Biology 12: 88-118.

15. Cooper A., D. Dryden (1984) Allostery without conformational change- A plausible Model European Biophysics Journal: 103-109.

16. Cui Q., M. Karplus, (2008) Allostery and cooperativity revisited. Protein Science 17: 1295-1307.

17. Motlagh H.N., J.O. Wrabl, J. Li, V.J. Hilser, (2014) The ensemble nature of allostery. Nature 508: 331-339.

18. Wooll J.O., R.H.E. Friesen, M.A. White, S.J. Watowich, R.O. Fox, et al. (2001) Structural and Functional Linkages Between Subunit Interfaces in Mammalian Pyruvate Kinase. Journal of Molecular Biology 312: 525-540.

19. Chung-Jung T., N. Ruth, (2014) A Unified View of "How Allostery Works". PLoS Computational Biology 10.